Manipulating Backbone Structure to Enhance Low Band Gap Polymer Photovoltaic Performance

ARTICLE *in* ADVANCED ENERGY MATERIALS · JULY 2013

Impact Factor: 16.15 · DOI: 10.1002/aenm.201300031

9 AUTHORS, INCLUDING:

Feng Liu
University of Massachusetts Amherst
160 PUBLICATIONS **2,636** CITATIONS
SEE PROFILE

Xia Guo
Soochow University (PRC)
71 PUBLICATIONS **3,826** CITATIONS
SEE PROFILE

Wei Zhang
The University of Manchester
121 PUBLICATIONS **883** CITATIONS
SEE PROFILE

Jianhui Hou
Chinese Academy of Sciences
148 PUBLICATIONS **12,312** CITATIONS
SEE PROFILE

ADVANCED ENERGY MATERIALS
www.advenergymat.de

Materials Views
www.MaterialsViews.com

Manipulating Backbone Structure to Enhance Low Band Gap Polymer Photovoltaic Performance

Ye Huang, Feng Liu, Xia Guo, Wei Zhang, Yu Gu, Jianping Zhang, Charles C. Han, Thomas P. Russell,* and Jianhui Hou**

A pair of polymers, PBDTBT and PBDTDTBT, was synthesized for application in polymer solar cells (PSCs). Although these two polymers have similar absorption bands and molecular energy levels, PBDTDTBT exhibits much better photovoltaic performance in polymer solar cell (PSC) devices with power conversion efficiency (PCE) of 7.4%. To understand the differences between PBDTDTBT and PBDTBT, we have investigated the correlations of the molecular structure, morphology, dynamics and efficiency of these two polymers. A theoretical investigation using density functional theory (DFT) and time-dependent DFT (TDDFT) has been employed to investigate the electron density and electron delocalization extent of the unimers. TEM data showed that PBDTDTBT phase separates from $PC_{71}BM$, while PBDTBT suffers from having a proper morphology on different processing conditions. Grazing incidence wide angle X-ray diffraction (GIWAXD) was used to probe the crystal structure of the polymers in thin film. A polymorph crystal structure was observed for PBDTBT. Grazing incidence small angle X-ray scattering (GISAXS) was used to probe the size scale of phase separation, with an optimized 25 nm feature size observed for PBDTDTBT/$PC_{71}BM$ blends, which agrees well with TEM results. Femtosecond transient absorption (TA) spectroscopy was used to probe the dynamics of the fundamental processes in organic photovoltaic (OPV) materials, such as charge separation and recombination. The enhanced absorption coefficient, good charge separation, optimal phase separation and higher charge mobility all contribute to the high PCE of the PBDTDTBT/$PC_{71}BM$ devices.

1. Introduction

Polymer based bulk heterojunction (BHJ) solar cells have attracted much interest due to their promising performance, thin device structure and cost-effective fabrication.[1] Over the past decades, significant progress has been made in both material development and device engineering and their power conversion efficiencies (PCE) have reached ~9%.[2] Currently, the low band gap conjugated polymer design protocol, by hybridizing the frontier orbitals of an electron rich unit (donor) and an electron deficient unit (acceptor), has been proven to be effective in modulating the optical band gap and energy levels, and has gained prominence in photovoltaic polymer design.[3,4] It has to be noted that, although significant progress has been made with low band gap polymers, there are still many conjugated polymers that have a low band gap nature but their devices perform poorly.[5,6] This discrepancy more than likely arises from the physical properties of the materials and the morphology of the active layer. In terms of electronic structure, it was pointed out that a "weak donor" and "strong acceptor" design could lead to deeper HOMO energy levels, thereby increasing the open circuit voltage in a device.[7] Yet, in this study, along with others, it was found that even polymers with similar structures and electronic energy levels can still behave quite differently in a device.[4,8] This necessitates a more detailed polymer design protocol, which integrates the intrinsic energy levels, optical properties, crystalline structure and morphological behavior. It is well known that the processing conditions, for example, the choice of solvents, the use of additives, and subsequent thermal annealing processes will strongly affect the BHJ morphology and the physical properties of materials.[9] Consequently, understanding the relationship between the polymer structure and morphology would significantly benefit the material design.

In this work, a pair of new polymers, Poly[4-(4,8-bis((2-hexyldecyl)oxy)benzo[1,2-*b*:4,5-*b'*]dithiophen-2-yl)-*alt*-benzo[*c*][1,2,5]thiadiazole] (**PBDTBT**) and Poly[4-(4-(2-ethylhexyl)-5-(8-((2-ethylhexyl)oxy)-4-((2-ethyloctyl)oxy)benzo[1,2-*b*:4,5-*b'*]dithiophen-2-yl)

Dr. Y. Huang, X. Guo, Prof. C. C. Han, Prof. J. Hou
Key Laboratory of Polymer Physics and Chemistry
Beijing National Laboratory for Molecular Sciences
Institute of Chemistry, Chinese Academy of Sciences
Beijing 100190, China
E-mail: hjhzlz@iccas.ac.cn
F Liu, Y. Gu, Prof. T. P. Russell
Department of Polymer Science and Engineering
University of Massachusetts
Amherst, Massachusetts 01003, USA
E-mail: russell@mail.pse.umass.edu
W. Zhang, Prof. J. Zhang
Department of Chemistry
Renmin University of China
Beijing, 100872, China
E-mail: jpzhang@chem.ruc.edu.cn

DOI: 10.1002/aenm.201300031

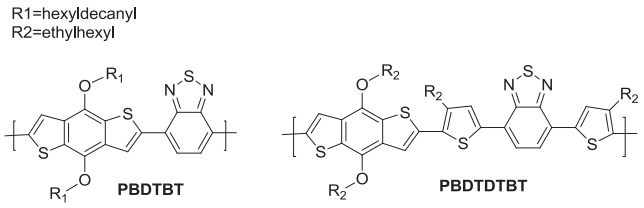

Scheme 1. Molecular structure of **PBDTBT** and **PBDTDTBT**.

thiophen-2-yl)-*alt*-7-(4-(2-ethylhexyl)thiophen-2-yl)benzo[*c*][1,2,5] thiadiazole] (**PBDTDTBT**) (shown in **Scheme 1**) were investigated. Studies were performed to characterize a broad range of properties of these materials, from the photovoltaic to opto-electronic, morphological and dynamical properties, so as to gain a rational design rule for photovoltaic polymers. It is worth mentioning that the two polymers used in this study have similar molecular structures and molecular energy levels, and are well-suited to elucidate changes in the structure–morphology–performance of materials induced by the minor structural change. Compared to **PBDTBT**, two thiophene units were introduced into **PBDTDTBT** as spacer groups. As the thiophene is a five-membered ring with small torsion angles and adjacent conjugated units, the incorporation of thiophene between the benzo[1,2-*b*:4,5-*b*']dithiophene (BDT) and benzo[*c*][1,2,5]thiadiazole (BT) units[10] will not change the planarity of the backbone, and result in good coplanarity of backbone units and increased electron delocalization in the solid state.[11] Ethylhexyl has been introduced to the 4-position of the thiophene bridge to enhance the processability of **PBDTDTBT**.[6] Although these two polymers exhibit similar absorption bands and molecular energy levels, **PBDTDTBT** blended with [6,6]-phenyl-C_{71}-butyric acid methyl ester ($PC_{71}BM$) exhibits much better photovoltaic performance, with a PCE up to 7.40% in PSC devices, in comparison to **PBDTBT** which has a PCE of 1.71%. To understand the difference in the efficiencies, we investigated the correlation between the structure, morphology, dynamics and efficiency of these two polymers. Density functional theory (DFT) and time-dependent DFT (TDDFT) were used to investigate the electron density and extent of electron delocalization of the repeat unit. Atomic force microscopy (AFM) and transmission electron microscopy (TEM) were used to identify the structural characteristics of the film, such as the phase-separated morphology. Femtosecond transient absorption (TA) spectroscopy was used to probe the dynamics of the fundamental processes in organic photovoltaic (OPV) materials, such as charge separation and recombination.

2. Results and Discussion

2.1. Optical Properties and Computational Study

The UV-vis spectra of the polymers in chloroform solution and in thin solid film are shown in **Figure 1**. For **PBDTBT**, a more electron rich aromatic BDT unit is directly linked to the electron accepting BT units, thus a stronger electron delocalization and frontier orbital hybridization is presented, leading to broad wavelength absorption. For **PBDTDTBT**, though the introduction of five-membered thiophene ring does not distort the geometry of the backbone significantly, it relieves the direct electron communication of BDT and BT units. From solution to thin film, solid-state packing leads to a better planarity of the backbone, which can be seen from the obvious red shift (around 40 nm). For **PBDTBT**, the solution to solid-state transition change is minor, indicating this polymer has a flat backbone, both in solution and in thin film. This planarity will lead to an easy packing of the polymer chains into crystals and, thus a higher degree of crystallinity would be expected. At the same time, we observed that the absorption coefficient of **PBDTDTBT** thin film is much higher than that of **PBDTBT** (Figure 1b). As a higher absorption coefficient usually leads to a better utilization of the sunlight, a larger J_{sc} would be expected. The UV-vis spectra of blends (with the same condition as device fabrication process) are shown in Figure 1c. DIO additive does not affect the light absorption spectrum of the **PBDTBT** blends, while an obvious long wavelength absorption enhancement is observed in the **PBDTDTBT** blends, indicating DIO enhances the ordering of the polymers in the blends.[12]

The difference in absorption coefficient primarily arises from the changes in the electronic structure of the polymers, due to the introduction of the thiophene units. To elucidate the origin of the absorption changes, time-dependent density functional theory (TDDFT)[13] at the B3LYP/6-31G(d,p) level has been used to gain insight into the vertical singlet (S_0-S_1) electronic transitions. Although both exhibit almost

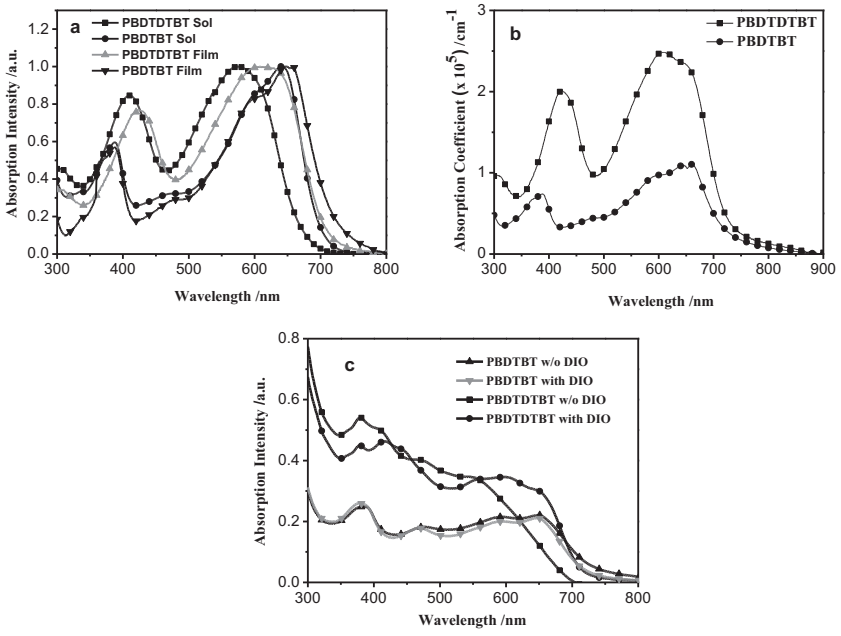

Figure 1. UV-vis absorption spectra of (a) all polymers in chloroform solution and in solid-film state on quartz, (b) the corresponding absorption coefficients and (c) blend films. (The fabrication process, including D/A ratio and spin coating rate, is same with device fabrication condition.)

Table 1. Basic properties (optical and electrochemical) of the pair polymers and hole mobilities of the polymers measured by space-charge-limited current (SCLC) method.[19]

Polymers	M_n/PDI [kg/mol]	λ_{max}(onset) [nm] thin film	α [cm^{-1}] thin film	E_g^{opt} [eV]	HOMO[a)] [eV]	LUMO[a)] [eV]
PBDTBT	54.4/3.7	380, 650 (740)	1.1×10^5	1.67	–5.22	–3.71
PBDTDTBT	82.2/4.3	425, 620 (720)	2.5×10^5	1.72	–5.24	–3.71

[a)]The HOMO and LUMO energy levels are measured by cyclic voltammetry method.

the same HOMO and LUMO levels by cyclic voltammetry (CV) measurements (see **Table 1** and Figure 1S in the Supporting Information), their electron structure in the frontier orbital are markedly different. A theoretical investigation using TDDFT[14] indicates that the HOMO→LUMO transition configurations predominantly arise from S_0-S_1 transitions for both cases. In **Figure 2**, the electron density in the LUMO wave function is more localized on the acceptor unit of BT or DTBT, while the electron density associated with the HOMO wave function remains delocalized over both the acceptor and donor units (also see Figure 2S in the Supporting Information). The localization of the LUMO decreases the orbital overlap with the HOMO, which can weaken the strength of the lowest S_0-S_1 absorption.[15] It is noted that the LUMO wave function of the polymer **PBDTBT**, where the thiophene bridge is absent, is more localized on the BT unit, while the HOMO wave function still remains well delocalized; The LUMO wave function of **PBDTDTBT**, on the other hand, is more delocalized over both the BT unit and the thiophene bridges. This should favor HOMO/LUMO overlap in **PBDTDTBT** and enhance the extinction coefficient for the lowest and dominated charge transfer (HOMO→LUMO) electronic excitation. As the oscillator strength is related to the experimental extinction coefficient,[16] **PBDTDTBT** has a much stronger oscillator strength than **PBDTBT**, which complements the extinction coefficient difference.[14,17] The oscillator strength of an electronic excitation is directly determined by the square of the transition dipole moment between the ground and excited state, which is a function of the spatial overlap between the ground-state and excited-state wave functions.[18] The amplitudes of calculated dipole moments for the unimers are also shown in **Table 2**.

Table 2. Calculated absorption of the unimers at TD-B3LYP level.

	State	λ(nm)/E(eV)	oscillator	Main configurations	Dipole moment
BDTBT	S_1	355.8/3.48	0.6854	HOMO→LUMO (79%)	1.47
BDTDTBT	S_1	453.9/2.73	1.2366	HOMO→LUMO (92%)	2.42

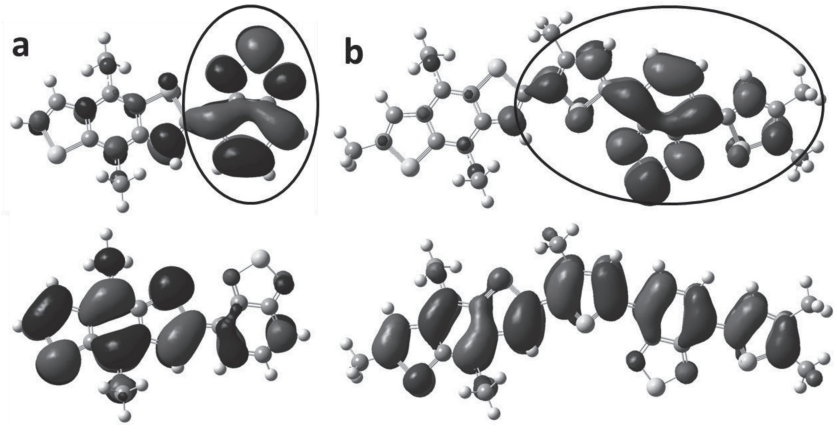

Figure 2. DFT-calculated LUMO (up) and HOMO (down) of the geometry optimized structures (B3LYP/6-31G*) of the unimers (a) **BDTBT** and (b) **BDTDTBT** unimer.

2.2. Photovoltaic Properties

The photovoltaic results of the PSC devices fabricated under the optimal conditions (donor/acceptor (D/A) ratio, solvents, thickness, etc. are listed in **Table 3**, and the corresponding *I-V* curves of these devices are shown in **Figure 3**. For the BHJ PSC devices based on **PBDTBT** and **PBDTDTBT** blended with $PC_{71}BM$ ([6,6]-phenyl C_{71}-butyric acid methyl ester), different D/A ratios were used to optimize the photovoltaic performance of the devices. For both polymers, optimal photovoltaic results were obtained from the devices with the D/A ratio of 1:1. DIO additive (1,8-diiodooctane (DIO)/DCB, v/v) was used to improve the performance of **PBDTDTBT**/$PC_{71}BM$ blends.[6] For **PBDTBT**/$PC_{71}BM$, it was found that the device performance with DIO is lower than the device without DIO. Figure 3 shows the *I-V* curves and external quantum efficiencies (EQE) for solar cells under illumination of AM 1.5G (100 mW/cm^2). Comparing their optimal device results, PCEs of 1.71% and 7.40% for **PBDTBT** and **PBDTDTBT**, respectively, were achieved. PSC devices based on these two polymers exhibit little difference in the open circuit voltages (V_{oc}), but **PBDTDTBT** shows a much larger short circuit current (J_{sc} = 13.56 mA/cm^2) and fill factor (FF = 69.10%) compared to **PBDTBT** (J_{sc} = 5.32 mA/cm^2 and FF = 42.31%). The EQE of **PBDTDTBT**/$PC_{71}BM$-based solar cells was as high as 71%, in comparison to the 29% EQE of the **PBDTBT**/$PC_{71}BM$-based solar cells, indicating a more efficient generation and transport of charge carriers in **PBDTDTBT**. The space charge limited current (SCLC) method[19] was used to evaluate the hole-mobility of the blend films. The

Table 3. Photovoltaic properties of PSCs based on the polymers.

Polymers	Polymer:$PC_{71}BM$ (w/w)	DIO (v%)	Thickness (nm)	V_{oc}(V)	J_{sc}(mA/cm^2)	*FF*(%)	PCE(%)	Hole Mobility (cm^2/V·s)
PBDTBT	1:1	0	70	0.76	5.32	42.31	1.71	4.77×10^{-6}
PBDTBT	1:1	3	65	0.76	4.87	41.73	1.55	N/A
PBDTDTBT	1:1	0	95	0.84	7.81	51.16	3.35	N/A
PBDTDTBT	1:1	3	100	0.79	13.56	69.10	7.40	1.42×10^{-2}

mobility obtained for **PBDTDTBT**/$PC_{71}BM$ blends was four orders of magnitude higher than that of **PBDTBT**/$PC_{71}BM$ blends (Table 3).

2.3. Morphology Characterization

Grazing incidence wide angle X-ray diffraction (GIWAXD) was used to measure the order of the polymers cast from DCB solutions. **Figure 4**a presents the out-of-plane GIXD profiles of **PBDTBT** and **PBDTDTBT** thin films. For **PBDTBT** sample, a strong (100) reflection peak at ~0.27 Å^{-1} was observed (corresponding to a d-spacing of 23.2 Å). **PBDTDTBT** shows a pronounced (100) reflection at ~0.36 Å^{-1}, corresponding to a d-spacing of 17.4 Å. the decrease (100) d-spacing is due to the short alkyl chain in the BDT unit. For the pure polymers, the GIXD out-of-plane profile of **PBDTDTBT** (See Figure 3S in the Supporting Information), shows a reflection at ~1.65 Å^{-1} (corresponding to a d-spacing of 3.8 Å, characteristic of the π-π stacking distance), indicating the chains adopt a mixed edge-on and face-on orientations. For **PBDTBT**, no clear reflection was seen in this scattering vector range, suggesting that these polymer chains adopt predominantly an edge-on orientation. The **PBDTDTBT**/$PC_{71}BM$ blend show an out-of-plan profile that is similar to the pure polymer, except a diffusive maximum arising from the PCBM is seen at 1.4 Å^{-1}. The **PBDTBT**/$PC_{71}BM$ blends show three orders of reflections of the (100) peak, indicating a good ordering of the polymer in the blends. It should also be noted that there is evidence of a shoulder in the (100) reflection for the PBDTBT. In fact, three Gaussian oscillators were needed to best fit the data. The major peak in the fitting yields a crystal size of ~20 nm for both blend samples. The contribution for the shoulder at ~0.32 Å^{-1} is enhanced when the DIO is used. Whether this data indicates the presence of a polymorphic crystal structure or a mixture of crystals with aggregates formed during preparation is not known at present and will be the subject of a future study. The low mobility in SCLC measurement can arise from the difference in the orientation of the chains, since the orientation can affect the efficiency of charge transport in the organic thin film devices where π–stack in a direction parallel to the substrate has been argued to be beneficial for the charge transport.[20] Yet, the nearly four orders of magnitude difference in the mobility for blended thin film suggest that, in **PBDTBT** blends, the crystallites may contain a substantial amount of disorder that will drastically reduce hole mobility.

The lateral phase separation information of the blends was accessed by using grazing incidence small angle X-ray scattering (GISAXS), as shown in Figure 4b. The **PBDTDTBT**/$PC_{71}BM$ blends without DIO exhibit a sharp upturn in the low*q* region indicating the presence of large size-scale heterogeneity in the blends. With the use of DIO, the **PBDTDTBT**/$PC_{71}BM$ blend showed a broad maximum at 0.02 Å^{-1} (~30 nm). This is reasonable, since **PBDTDTBT** is crystalline in the thin films and the maximum is characteristic of the average size of the crystalline domains. It should be noted that if the **PBDTDTBT** blend solutions (10 mg in DCB) are left undisturbed for several days, the formation of a gel-like structure can be observed, suggesting that **PBDTDTBT** can form fibrils in concentrated solutions. Consequently, during film preparation, such fibril aggregates can form in solution and be deposited in the film, forming a network-like morphology where, with subsequent solvent evaporation, a PCBM-polymer mixture is deposited within this fibrillar network.[21] The presence of DIO, which accelerates fibril formation during solution casting, can lead to the formation of a network-like fibrillar structure at higher solvent concentrations and, therefore, a slightly larger or more open network. In the case of **PBDTBT**/$PC_{71}BM$ blends without DIO, no obvious phase separation on the tens of nanometer length scale was observed. While **PBDTBT** crystals are obviously present, the strong upturn observed in the low *q* region indicates that phase separation on a large length scale has occurred. However, in the case of **PBDTBT**/$PC_{71}BM$ blends with DIO, a broad maximum at ~0.007 A^{-1} is seen, indicating domain sizes of ~90 nm, which is not optimal for device performance.

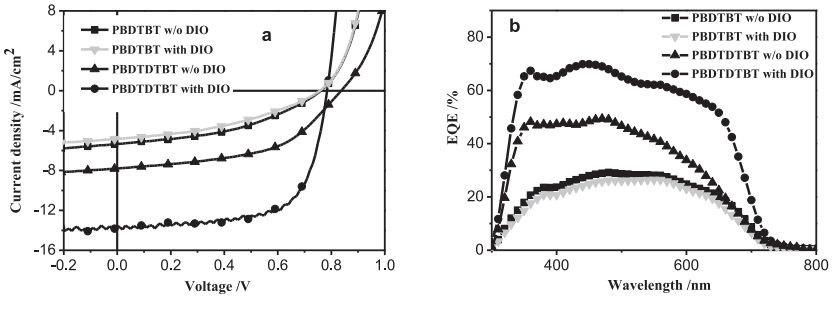

Figure 3. (a) *I-V* characteristics of the devices with the structure of ITO/PEDOT:PSS/polymer:$PC_{71}BM$/Ca/Al under the illumination of AM 1.5G from a solar simulator.(100 mW/cm^{-2}). (b) EQE curves of the corresponding polymer solar cells.

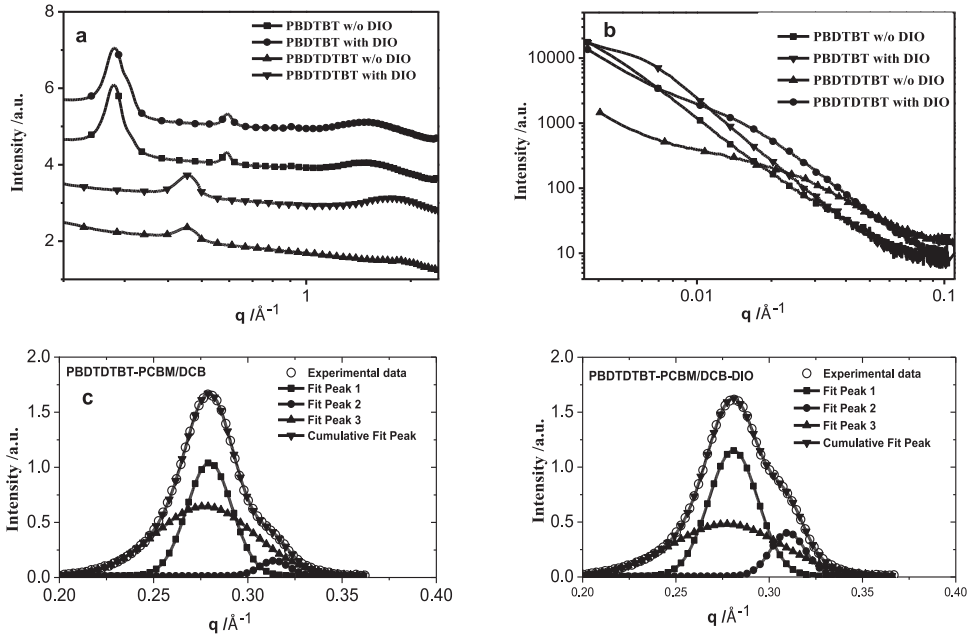

Figure 4. The GIXD profiles are (a) out-of-plane GIWAXD curves for thin blends films of **PBDTBT** and **PBDTDTBT** with an incidence angle of 0.2°; (b) in-plane GISAXS curves for the blends films. These curves were taken in a direction normal to the substrate surface, and (c) Gaussian fitting for the GIWAXD data. The preparation conditions of the blends are consistent with the optimal device fabrication process.

TEM can be used to probe the real-space, nanometer-scale morphology of thin films (**Figure 5**). For the **PBDTBT** blends without DIO (Figure 5a), a diffuse, ill-defined image was obtained, providing little information of the morphology. For **PBDTBT** thin films using DIO (Figure 5b), well-defined dark and bright areas can be seen. The dark area is PCBM-rich, while the bright areas are crystals. Their size scale agrees well with both the GISAXS and GIWAXD results. The bright, crystalline areas show fibrillar textures and either crystalline aggregates or plate-like regions. From the different TEM images, along with the absorption, device and Xray studies, we can conclude that, in the **PBDTBT**/PCBM blends, DIO accelerates the ordering of the **PBDTBT** and the consequent phase-separated morphology. While **PBDTBT** is highly crystalline in nature, the preferential solubility of PCBM and insolubility of **PBDTBT** in DIO prevent the PCBM from interfering with the ordering of the **PBDTBT**, giving rise to the formation of well-defined crystalline textures in the thin films, forming a crystalline network with sharp boundaries in which the remaining **PBDTBT** and PCBM are deposited. This is consistent with the generally-accepted role of the additive in sample preparation.[22] The active layer of **PBDTDTBT** blends, processed without DIO, contains large fullerene clusters that

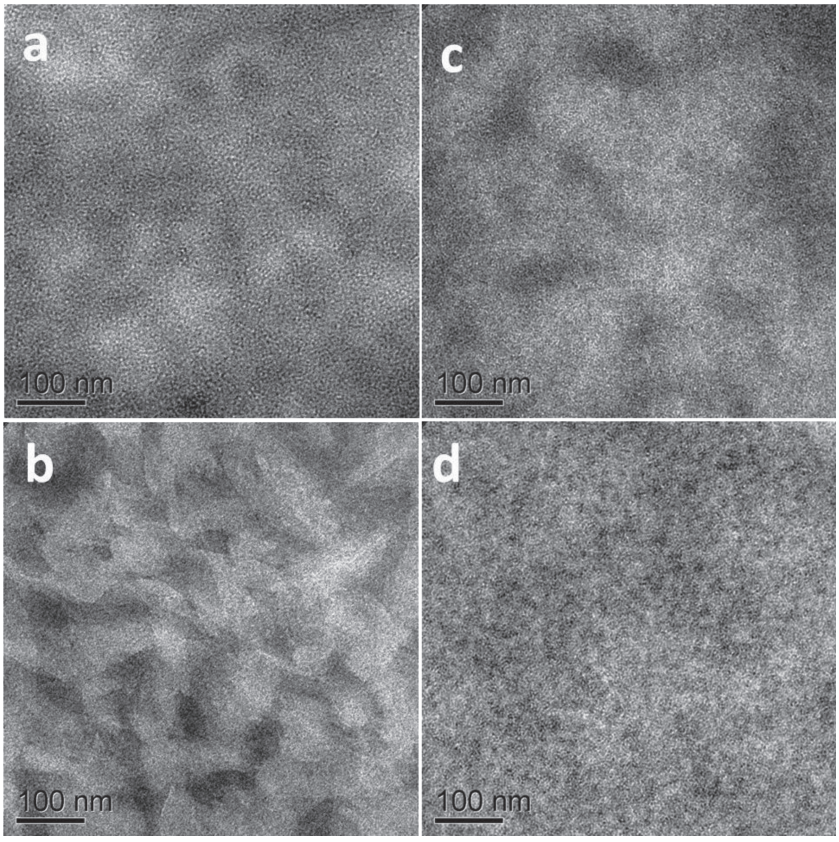

Figure 5. TEM images: (a) **PBDTBT**:$PC_{71}BM$ (1:1, w/w) and (b) **PBDTBT**:$PC_{71}BM$ (1:1, w/w) containing 3 vol% of DIO; (c) **PBDTDTBT**:$PC_{71}BM$ (1:1, w/w) and (d) **PBDTDTBT**:$PC_{71}BM$ (1:1, w/w) containing 3 vol% of DIO, respectively. (The scale bar is 100 nm).

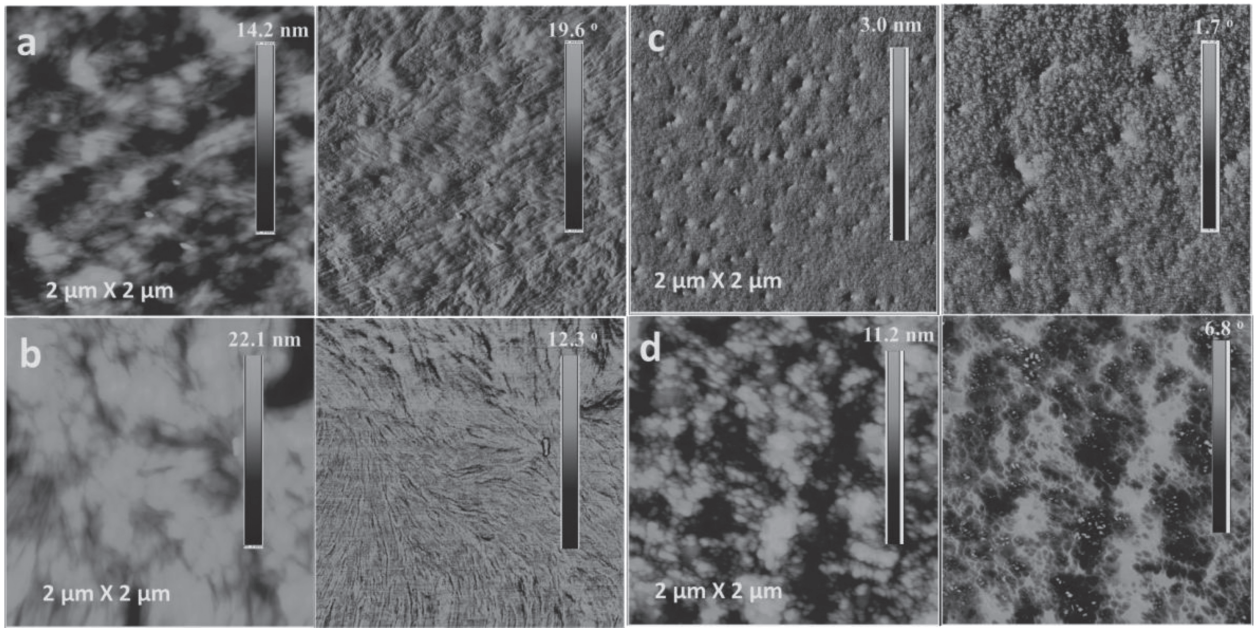

Figure 6. AFM images: left are height images and right are phase images for (a) **PBDTBT**:$PC_{71}BM$ (1:1, w/w) and (b) **PBDTBT**:$PC_{71}BM$ (1:1, w/w) containing 3 vol% of DIO; (c) **PBDTDTBT**:$PC_{71}BM$ (1:1, w/w) and (d) **PBDTDTBT**:$PC_{71}BM$ (1:1, w/w) containing 3 vol% of DIO, respectively.

are evidenced as dark regions in the bright-field TEM image (Figure 5c). In active layers processed with DIO, the phase separated morphology on the ~10 nm length scale is observed, leading to good device performance. Atomic force microscopy (AFM) was used to assess the surface morphology of the active layer. The height and phase images of the polymer blends prepared using the same process as those used in PSC devices are shown in **Figure 6**. Comparing Figure 6a and Figure 6b, the surface morphology of the **PBDTBT** active layer with DIO contains bundles of nanofibrils. This high polymer content at the surface (or interface with the electrode in the device) reduces effective electron collection, thus yielding a poor device performance. The surface of the **PBDTDTBT** active layer prepared without DIO is quite smooth with minor defects. With the use of DIO, the surface becomes rough on the nanoscopic length scale and, in the phase image, an open fibrilar network is evident, leading to an enhanced performance.

2.4. Dynamics of Charge Separation and Recombination

It is well-accepted that BHJ solar cells involve multistep processes, including exciton generation, diffusion, charge separation, carrier generation, and transportation. Femtosecond time-resolved absorption (TA) spectroscopy was used to examine the primary exciton and polaron dynamics, which are directly related to carrier mobility and film morphology. TA spectra of the blends films of **PBDTDTBT** (with DIO) and **PBDTBT** (without DIO) mixed with $PC_{71}BM$ (which is the same condition used for the optimal devices) in the NIR region of 850-1350 nm were measured, respectively (**Figure 7**a and Figure 7b). In transient absorption, the 1300 nm band is dominated by the excited-state absorption, i.e., the absorptive transition from the lowest singlet exciton to a higher-lying exciton state ($S_1 \rightarrow S_n$), whereas the 1000 nm band can be attributed mainly to the absorption of polarons.[23] Optical densities in different time frames were measured. From 100 ps to 1700 ps, little polaron decay is seen in the spectra of the **PBDTDTBT** blends, whereas very fast polaron decay is observed for the **PBDTBT** blends. Inspecting the corresponding decay kinetics in Figure 7c, it can be inferred from the 1200-nm kinetics that the decay time for exciton diffusion to the interface of **PBDTDTBT**/$PC_{71}BM$ blends is about 3.00 ps, while that for the **PBDTBT**/$PC_{71}BM$ blends is 1.47 ps. The longer timescale of exciton diffusion for the **PBDTDTBT** blends can be explained by the larger domain size in the **PBDTDTBT** blends (Figure 6d) than for the **PBDTBT** blends (Figure 6a). Based on GISAXS and TEM data, a 25 nm size scale phase separation is observed for **PBDTDTBT** and no obvious phase separation on this size scale or smaller is observed for **PBDTBT**, which may arise from the good miscibility of the polymer and PCBM. However, the difference in the exciton diffusion time scales is not enough to give rise to the large difference in the device performance; since on such short time scale, the loss of excitons due to relaxation to the ground state is virtually negligible for both blends. This relation was used to model the recombination behavior of the polarons. To avoid interference from the excitons, we examined the 1000-nm kinetics in the time frame of 100~1700 ps. The results show that the recombination of **PBDTBT**/$PC_{71}BM$ blends ($\tau = 1.8$ ns) is much faster than that of **PBDTDTBT**/$PC_{71}BM$ blends (τ = long), which means that the loss of charges via recombination in **PBDTBT**/$PC_{71}BM$ blends is more serious than that in **PBDTDTBT**/$PC_{71}BM$ blends. (The decay of the 1000-nm polaron kinetics is assumed to be due to the geminate recombination under the low photon fluence excitation used here.) This is understandable in viewing the

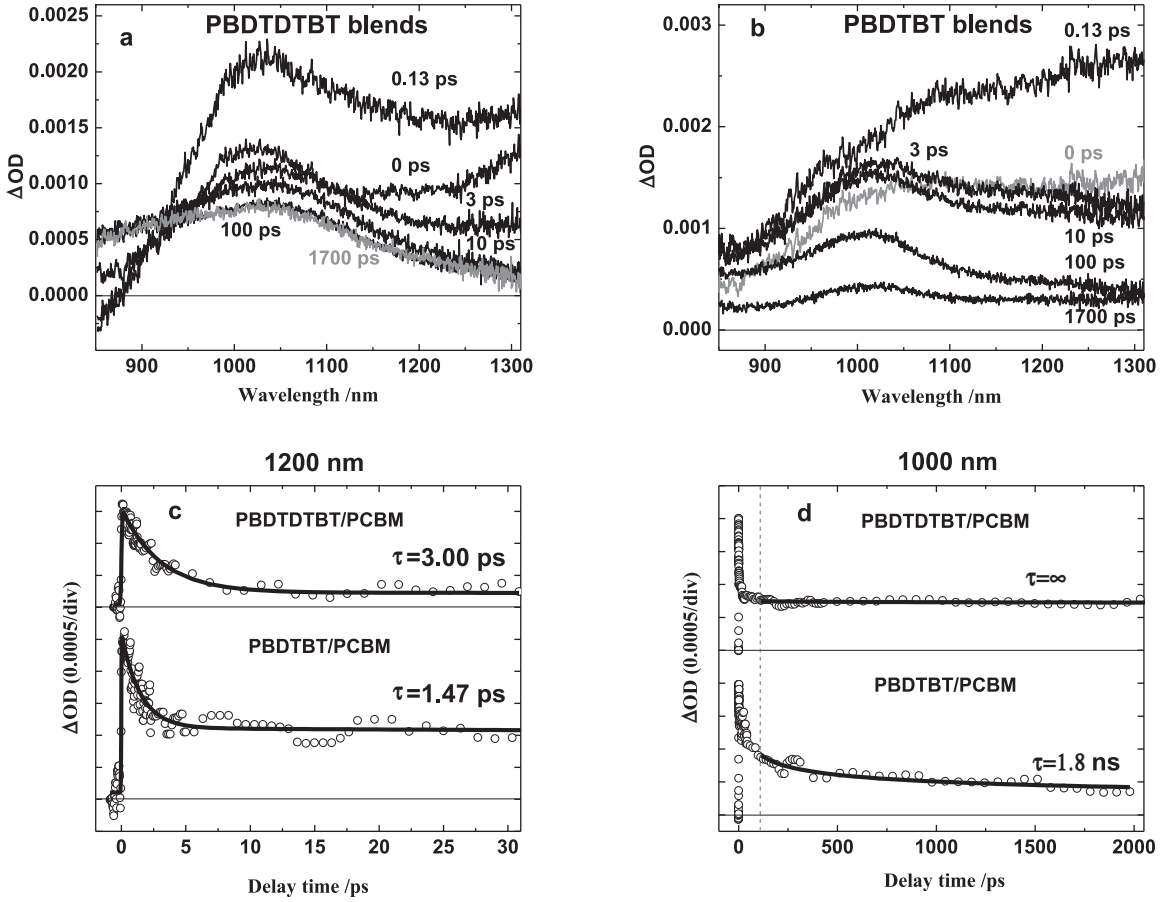

Figure 7. Transient spectra at the indicated delay times recorded after photoexcitation at 680 nm for a) **PBDTDTBT**/$PC_{71}BM$ (2.1×10^{13} photons·cm^{-2}·$pulse^{-1}$) and b) **PBDTBT**/$PC_{71}BM$ (2.1×10^{13} photons·cm^{-2}·$pulse^{-1}$). (c, d) Kinetic traces at the indicated probing wavelengths plotted from the corresponding spectral sets of the **PBDTDTBT**/$PC_{71}BM$ and **PBDTBT**/$PC_{71}BM$ films. Solid lines for the 1200-nm kinetics are fitting curves based on the model function $\Delta OD = A\cdot\exp(-t/\tau)+B\cdot\exp(-t/\infty)$, and those for the 1000-nm kinetics (100 – 2000 ps) are fitting curves based on the $\Delta OD = A\cdot\exp(-t/\tau)$. (The blends film compositions and preparations were consistent with those generally used in optimized solar cells).

difference in the domain sizes of the two different blend films. In addition, the four orders of magnitude larger hole mobility of **PBDTDTBT**/$PC_{71}BM$ blends with respect to **PBDTBT**/$PC_{71}BM$ blends facilitates a higher e^--h^+ escape probability in the **PBDTDTBT**/$PC_{71}BM$ blend films, while reducing the loss of charges via germinate recombination.[24] Therefore, the results of the ultrafast exciton and charge dynamics complement the results of the morphology and the hole mobility characterization, which together explain the significant differences in J_{sc},*FF* and PCE of the devices based on the two polymers. The fast recombination rate at the interface becomes one of the key factors in limiting the efficiency of **PBDTBT**.

3. Conclusions

In summary, a pair of polymers **PBDTBT** and **PBDTDTBT** was synthesized and high performance BHJ solar cells were achieved in **PBDTDTBT** based PSCs. The only difference in molecular structure aspect between **PBDTBT** and **PBDTDTBT** is the thiophene bridge in between the BDT and BT unit. The J_{sc} and *FF* of **PBDTDTBT-**based devices are much larger than those of **PBDTBT**. Our studies correlating the molecular structure, thin film morphology, hole mobility, dynamics and efficiency revealed several important factors that contribute to the high J_{sc},*FF* and, therefore, PCE in **PBDTDTBT**. Optimizing **PBDTDTBT** from these aspects contribute to a much enhanced efficiency (up to 7.40%), significantly higher than that of **PBDTBT** based device (1.71%). Our study reinforces the importance of high absorption coefficient, a proper phase separated morphology, and a balance of maximal exciton separation and minimal charge recombination, while providing effective ways to predict and analyze the properties and potential of materials. We believe that these approaches should be considered and applied for future design of polymer solar cell applications.

Supporting Information

Supporting Information is available from the Wiley Online Library or from the author.

Acknowledgements

The authors would like to acknowledge the financial support from the Ministry of Science and Technology of the People's Republic of China (2011DFG63460 and 2011AA050523), National Natural Science Foundation of China (NSFC) (Nos., 51173189, 21104088) and Chinese Academy of Sciences (KJ2D-EW-J01). Feng Liu and Yu Gu were supported by Polymer-Based Materials for Harvesting Solar Energy, an Energy Frontier Research Center funded by the U.S. Department of Energy, Office of Science, Office of Basic Energy Sciences under contract DE-SC0001087 and the U.S. Department of Energy, Office of Basic Energy Sciences under contract DOE-DE-FG02-45612 (TPR).

Received: January 10, 2013
Published online: April 2, 2013

[1] a) G. Yu, J. Gao, J. C. Hummelen, F. Wudl, A. J. Heeger, *Science* **1995**, *270*, 1789; b) B. C. Thompson, J. M. J. Frechet, *Angew. Chem. Int. Edit.* **2008**, *47*, 58.

[2] a) Z. C. He, C. M. Zhong, X. Huang, W. Y. Wong, H. B. Wu, L. W. Chen, S. J. Su, Y. Cao, *Adv. Mater.* **2011**, *23*, 4636; b) H. Y. Chen, J. H. Hou, S. Q. Zhang, Y. Y. Liang, G. W. Yang, Y. Yang, L. P. Yu, Y. Wu, G. Li, *Nat. Photon.* **2009**, *3*, 649; c) L. T. Dou, J. B. You, J. Yang, C. C. Chen, Y. J. He, S. Murase, T. Moriarty, K. Emery, G. Li, Y. Yang, *Nat. Photon.* **2012**, *6*, 180; d) Y. Huang, X. Guo, F. Liu, L. Huo, Y. Chen, T. P. Russell, C. C. Han, Y. Li, J. Hou, *Adv. Mater.* **2012**, *24*, 3383; e) Z. C. He, C. M. Zhong, S. J. Su, M. Xu, H. B. Wu, Y. Cao, *Nat. Photon*. **2012**, *6*, 591.

[3] a) Y. Y. Liang, L. P. Yu, *Acc. Chem. Res.* **2010**, *43*, 1227; J. H. Hou, H. Y. Chen, S. Q. Zhang, R. I. Chen, Y. Yang, Y. Wu, G. Li, *J. Am. Chem. Soc.* **2009**, *131*, 15586; b) S. Gunes, H. Neugebauer, N. S. Sariciftci, *Chem. Rev.* **2007**, *107*, 1324; c) J. C. Bijleveld, M. Shahid, J. Gilot, M. M. Wienk, R. A. J. Janssen, *Adv Funct. Mater.* **2009**, *19*, 3262; d) Y. Huang, L. J. Huo, S. Q. Zhang, X. Guo, C. C. Han, Y. F. Li, J. H. Hou, *Chem. Commun.* **2011**, *47*, 8904; e) Y. Huang, M. Q. Zhang, L. Ye, X. Guo, C. C. Han, Y. F. Li, J. H. Hou, *J. Mater. Chem.* **2012**, *22*, 5700.

[4] L. J. Huo, S. Q. Zhang, X. Guo, F. Xu, Y. F. Li, J. H. Hou, *Angew. Chem. Int. Edit.* **2011**, *50*, 9697.

[5] J. H. Hou, T. L. Chen, S. Q. Zhang, H. Y. Chen, Y. Yang, *J. Phys. Chem. C* **2009**, *113*, 1601.

[6] H. X. Zhou, L. Q. Yang, S. Q. Xiao, S. B. Liu, W. You, *Macromolecules* **2010**, *43*, 811.

[7] H. X. Zhou, L. Q. Yang, S. Stoneking, W. You, *ACS. Appl. Mater. Inter.* **2010**, *2*, 1377.

[8] C. Piliego, T. W. Holcombe, J. D. Douglas, C. H. Woo, P. M. Beaujuge, J. M. J. Frechet, *J. Am. Chem. Soc.* **2010**, *132*, 7595.

[9] F. Liu, Y. Gu, J. W. Jung, W. H. Jo, T. P. Russell, *J. Polym. Sci. Pol. Phys.* **2012**, *50*, 1018.

[10] J. H. Hou, M. H. Park, S. Q. Zhang, Y. Yao, L. M. Chen, J. H. Li, Y. Yang, *Macromolecules* **2008**, *41*, 6012.

[11] S. C. Price, A. C. Stuart, W. You, *Macromolecules* **2010**, *43*, 4609.

[12] a) J. T. Rogers, K. Schmidt, M. F. Toney, G. C. Bazan, E. J. Kramer, *J. Am. Chem. Soc.* **2012**, *134*, 2884; b) J. Peet, J. Y. Kim, N. E. Coates, W. L. Ma, D. Moses, A. J. Heeger, G. C. Bazan, *Nat. Mater.* **2007**, *6*, 497.

[13] a) H. Y. Chen, J. H. Hou, A. E. Hayden, H. Yang, K. N. Houk, Y. Yang, *Adv. Mater.* **2010**, *22*, 371; b) N. Banerji, E. Gagnon, P. Y. Morgantin, S. Valouch, A. R. Mohebbi, J. H. Seo, M. Leclerc, A. J. Heeger, *J. Phys. Chem. C* **2012**, *116*, 11456; c) C. Risko, M. D. McGehee, J. L. Bredas, *Chem. Sci.* **2011**, *2*, 1200; d) B. P. Karsten, L. Viani, J. Gierschner, J. Cornil, R. A. J. Janssen, *J. Phys. Chem. A* **2008**, *112*, 10764.

[14] G. Garcia, A. Garzon, J. M. Granadino-Roldan, M. Moral, A. Navarro, M. Fernandez-Gomez, *J. Phys. Chem. C* **2011**, *115*, 6922.

[15] S. W. Ko, R. Mondal, C. Risko, J. K. Lee, S. H. Hong, M. D. McGehee, J. L. Bredas, Z. A. Bao, *Macromolecules* **2010**, *43*, 6685.

[16] V. J. Hammond, W. C. Price, *Trans. Faraday Soc.* **1955**, *51*, 605.

[17] J. Ku, Y. Lansac, Y. H. Jang, *J. Phys. Chem. C* **2011**, *115*, 21508; B. Carsten, J. M. Szarko, H. J. Son, W. Wang, L. Y. Lu, F. He, B. S. Rolczynski, S. J. Lou, L. X. Chen, L. P. Yu, *J. Am. Chem. Soc.* **2011**, *133*, 20468.

[18] L. Pandey, C. Risko, J. E. Norton, J. L. Bredas, *Macromolecules* **2012**, *45*, 6405.

[19] G. G. Malliaras, J. R. Salem, P. J. Brock, C. Scott, *Phys. Rev. B* **1998**, *58*, 13411; H. C. F. Martens, H. B. Brom, P. W. M. Blom, *Phys Rev B* **1999**, *60*, R8489.

[20] I. McCulloch, Martin Heeney, Clare Bailey, Kristijonas Genevicius, Iain MacDonald, Maxim Shkunov, David Sparrowe, Steve Tierney, Robert Wagner, Weimin Zhang, Michael L. Chabinyc, R. Joseph Kline, Michael D. McGehee, M. F. Toney, *Nat. Mater.* **2006**, *5*, 328.

[21] Y. Huang, H. Cheng, C. C. Han, *Macromolecules* **2011**, *44*, 5020; Y. Huang, H. Cheng, C. C. Han, *Macromolecules* **2010**, *43*, 10031.

[22] F. Liu, Y. Gu, C. Wang, W. Zhao, D. Chen, A. L. Briseno, T. P. Russell, *Adv. Mater.* **2012**, *24*, 3947.

[23] W. Zhang, R. Hu, D. Li, M. M. Huo, X. C. Ai, J. P. Zhang, *J. Phys. Chem. C* **2012**, *116*, 4298; M. Westerling, H. Aarnio, R. Osterbacka, H. Stubb, S. M. King, A. P. Monkman, M. R. Andersson, K. Jespersen, T. Kesti, A. Yartsev, V. Sundstrom, *Phys. Rev. B* **2007**, 75.

[24] V. D. Mihailetchi, L. J. A. Koster, J. C. Hummelen, P. W. M. Blom, *Phys. Rev. Lett.* **2004**, 93.